High-Performance Ultrathin Active Chiral Metamaterials

Zilong Wu[1], Xiaodong Chen[2], Mingsong Wang[1], Jianwen Dong[2] and Yuebing Zheng[1]*

[1] Department of Mechanical Engineering, Materials Science and Engineering Program, and

Texas Materials Institute

The University of Texas at Austin, Austin, Texas 78712, United States

[2] School of Physics & State Key Laboratory of Optoelectronic Materials and Technologies, Sun

Yat-sen University, Guangzhou 510275, China

E-mail: zheng@austin.utexas.edu

1. Dependence of Circular Dichroism (CD) on in-plane Rotation Angles between Top and Bottom Au Nanohole Arrays.
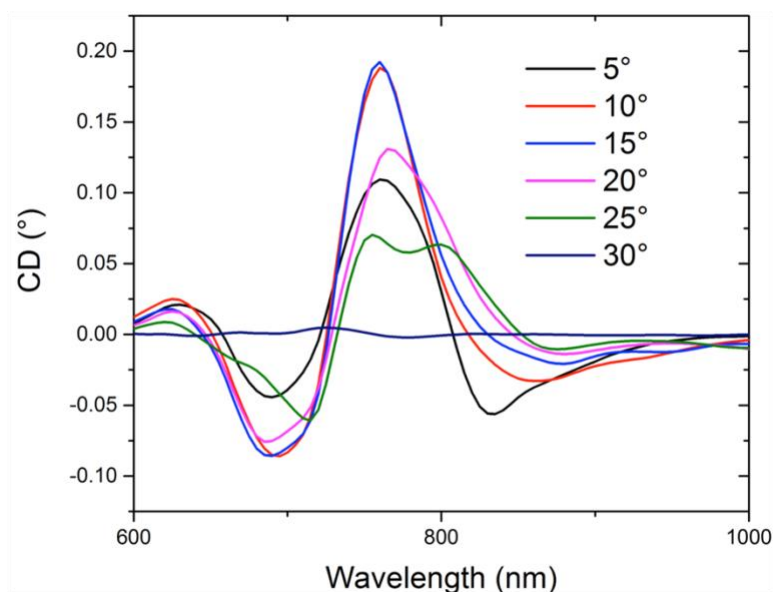

Figure S1. Simulated CD spectra of the right-handed MCMs with different in-plane rotation angles

between top and bottom Au nanohole arrays. The period and the thickness of the Au nanohole arrays were 300 nm and 60 nm, respectively. The thickness of the dielectric spacer was 30 nm.

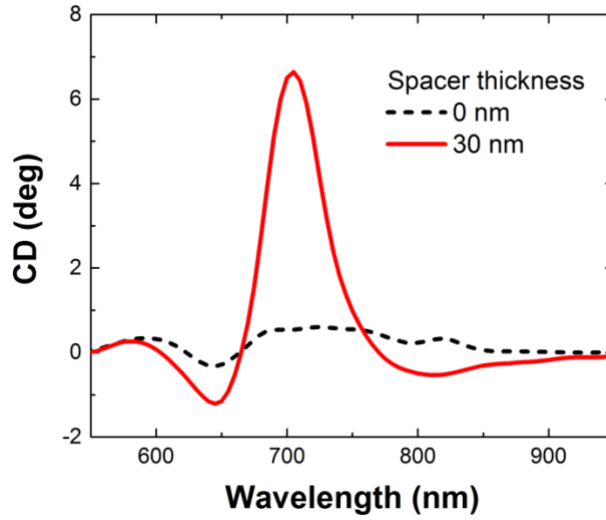## 2. Enhanced Optical Chirality by the Existence of Dielectric Spacer

Figure S2. Simulated CD spectra of the right-handed MCMs without spacer (dashed curve) and with a 30 nm dielectric spacer (solid curve). The period and the thickness of the Au nanohole arrays were 300 nm and 60 nm, respectively. The in-plane rotation angle between top and bottom Au nanohole arrays was 15°.

3. Fano Resonance

In plasmonic systems with Fano coupling between bright and dark modes, two pathways need to be considered. One is the direct excitation of the continuum of radiative waves. The other one is the excitation of the nanoradiative mode through its coupling to the continuum.[1] The Fano-like symmetric line shape induced by interference of these two pathways can be described as:

$$\sigma_s(\omega) = \frac{a^2}{\left(\frac{\omega^2 - \omega_s^2}{2W_s\omega_s}\right)^2 + 1} \qquad (S1)$$

where a, ω_s and W_s are the maximum resonance amplitude, the central spectral position and spectral width of the symmetric resonance, respectively. The asymmetric resonance in the Fano model can be obtain by:

$$\sigma_a(\omega) = \frac{\left(\frac{\omega^2 - \omega_a^2}{2W_a\omega_a} + q\right)^2 + b}{\left(\frac{\omega^2 - \omega_a^2}{2W_a\omega_a}\right)^2 + 1} \qquad (S2)$$

where ω_a and W_a are the central spectral position and spectral width of the asymmetric resonance, respectively. q and b are the asymmetric parameter and the modulation damping parameter in Fano resonances, respectively. The combination of the asymmetric resonance and symmetric resonance can be used to fit various spectra including scattering, transmission, and reflection. The analytical function is given by:

$$\sigma_t(\omega) = \sigma_s(\omega)\sigma_a(\omega) \qquad (S3)$$

In our case, the transmission spectra of the MCMs can be analytically fitted using Equation S3, as shown in Figure 2 and 3. The parameters for the Fano fitting in Figure 2 and 3 are given in Table S1 and S2, respectively.

Table S1. Parameters for the Fano fitting in Figure 2

	ω_a (10^{14} Hz)	W_a (10^{14} Hz)	ω_s (10^{14} Hz)	W_s (10^{14} Hz)	q	b	a
RCP	4.29	2.35	4.15	3.1	0.095	0.205	1.028
Linear	4.28	2.25	4.15	3.2	0.07	0.38	0.92
LCP	4.25	2.1	4.12	4.2	0.02	0.75	0.746

Table S2. Parameters for the Fano fitting in Figure 3 and the corresponding dephasing time of the Fano dip

	ω_a (10^{14} Hz)	W_a (10^{14} Hz)	ω_s (10^{14} Hz)	W_s (10^{14} Hz)	q	b	a	Dephasing time (fs)
20 nm	4.05	1.8	4.18	4.3	-0.12	0.26	0.8	11
30 nm	4.29	2.35	4.15	3.1	0.095	0.205	1.028	8.5
40 nm	4.39	2.4	4.11	2.95	0.19	0.38	1.026	8.3
50 nm	4.41	2.15	4.10	2.75	0.25	0.545	1.01	9.4

4. Coupled Oscillator Model

In coupled oscillator model, the behaviors of the bright mode and the dark mode can be described as:[2]

$$\omega_r^{-2}\ddot{p}(t) + \gamma_r\omega_r^{-1}\dot{p}(t) + p(t) = f(t) - \tilde{\kappa}q(t) \qquad (S4)$$

$$\omega_d^{-2}\ddot{q}(t) + \gamma_d\omega_d^{-1}\dot{q}(t) + q(t) = -\tilde{\kappa}p(t) \qquad (S5)$$

where $p(t)$, ω_b, and γ_b are the excitation, resonance frequency, and damping factor of the bright mode, respectively. $q(t)$, ω_d, and γ_d are the excitation, resonance frequency, and damping factor of the dark mode, respectively. $f(t)$ is the external force that excites the bright mode. The coupling strength between the bright and the dark modes is described as a constant $\tilde{\kappa}$. Solving the Equations S4 and S5 gives the following solutions:

$$p(t) = e^{-i\theta}P(\omega)e^{-i(\omega t)} \qquad (S6)$$

$$q(t) = e^{-i\phi}Q(\omega)e^{-i(\omega t)} \qquad (S7)$$

A phase shift between the bright and dark mode is considered in the complex coupling constant $\tilde{\kappa} = \kappa e^{-i(\theta-\phi)}$. From Equations S4-S7, we can obtain expressions in frequency domain:

$$P(\omega)e^{-i\theta} = \frac{F(\omega) - \tilde{\kappa}Q(\omega)e^{-i\phi}}{D_r} \qquad (S8)$$

$$Q(\omega)e^{-i\theta} = \frac{-\tilde{\kappa}P(\omega)e^{-i\phi}}{D_d} \qquad (S9)$$

where $D_d = 1 - \left(\frac{\omega}{\omega_d}\right)^2 - i\gamma_d\frac{\omega}{\omega_d}$ and $D_r = 1 - \left(\frac{\omega}{\omega_r}\right)^2 - i\gamma_r\frac{\omega}{\omega_r}$.

Considering the fact that transmission from plasmonic nanohole arrays is the result of scattered light by the sub-wavelength apertures,[3-4] we can analytically fit the transmission spectra of the MCMs through:

$$Transmission \propto \sigma_{scat} \propto \omega^4|P(\omega)|^2 \propto \left|\frac{\omega^2 D_d}{D_d D_r \omega_r^2 - \omega^2\kappa^2 e^{-2i(\theta-\phi)}}\right|^2 \qquad (S10)$$

Table S3 and S4 show the parameters for coupled oscillator model used in the fitting in Figure 2 and 3, respectively.

Table S3. Parameters for the fitting in Figure 2 based on coupled oscillator model

	ω_d (10^{14} Hz)	γ_d (x 10^{-2})	ω_r (10^{14} Hz)	γ_r (x 10^{-2})	κ (x 10^{-2})	θ - ϕ (x π)
RCP	4.29	5.59	3.87	37.2	10.0	1.035
Linear	4.28	6.07	3.85	39.0	6.50	1.055
LCP	4.28	4.67	3.84	39.1	1.87	0.9

Table S4. Parameters for the fitting in Figure 3 based on coupled oscillator model

	ω_d (10^{14} Hz)	γ_d (x 10^{-2})	ω_r (10^{14} Hz)	γ_r (x 10^{-2})	κ (x 10^{-2})	θ - ϕ (x π)
20 nm	4.09	6.85	3.89	36.5	12.7	1.03
30 nm	4.29	5.59	3.87	37.2	10.0	1.035
40 nm	4.37	9.15	3.93	30.5	7.78	1.02
50 nm	4.38	6.85	3.92	30.6	3.31	0.99

5. Scattering and Absorption Spectra

Scattering and absorption extinction spectra were simulated using FDTD, as shown in Figure S3. The scattering was obtained by an electromagnetic monitor located outside of the total-field scattered-field (TFSF) source, so that only scattered light is captured. The absorption was obtained by $A=1-T-R$, where T and R are the transmission and reflection by the MCMs, respectively.
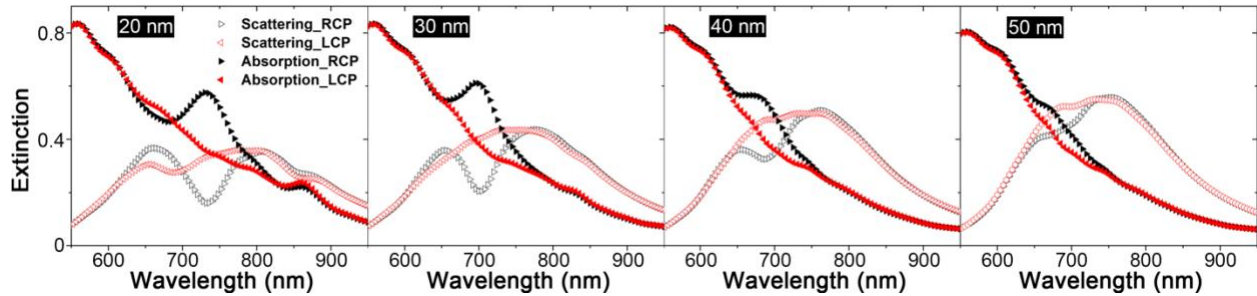

Figure S3. Simulated scattering and absorption spectra under LCP and RCP incident light for RH MCMs with variable spacer thickness. The in-plane rotation angle between top and bottom Au

nanohole arrays was 15°.

5. Fabrication of Chiral Metamaterials that Support Fano Resonances

We combined nanosphere lithography (NSL) and a wet-chemical transfer process to fabricate the moiré chiral metamaterials with precisely controlled dielectric spacer layers. As illustrated in "Process 1" of Figure S4, the polystyrene (PS) spheres with a diameter of 300 nm were self-assembled into a closed-packed monolayer and transferred onto a Cu sacrifice layer (~100 nm in thickness) on a glass substrate. The PS spheres were reduced by O_2 reactive ion etching (RIE). Deposition of Au followed by selective removal of the PS spheres (by ultrasonication in toluene) led to Au nanohole arrays on the Cu layer. A ~400 nm thin layer of polymethyl methacrylate (PMMA) was spin-coated on top of the Au nanohole arrays as a support layer for the wet-chemical transfer. A Cu etchant was used to selectively etch away the Cu layer, leaving the Au nanohole arrays and the PMMA layer floating on the solvent surface. In "Process 2" of Figure S4, another layer of Au nanohole arrays was fabricated directly on a glass substrate using NSL. A thin layer of spin-on glass (IC1) was coated on the Au nanohole array. The initial thickness of the as-prepared IC1 layer was ~180 nm. An SF_6 RIE was applied to control the thickness of the IC1 layer. At a targeted IC1 thickness, the floating layer of Au nanohole arrays and PMMA from Process 1 was transferred onto the top of the IC1 layer of desired thickness. The selective removal of the PMMA layer led to the MCM with the IC1 dielectric spacer layer on the glass substrate.
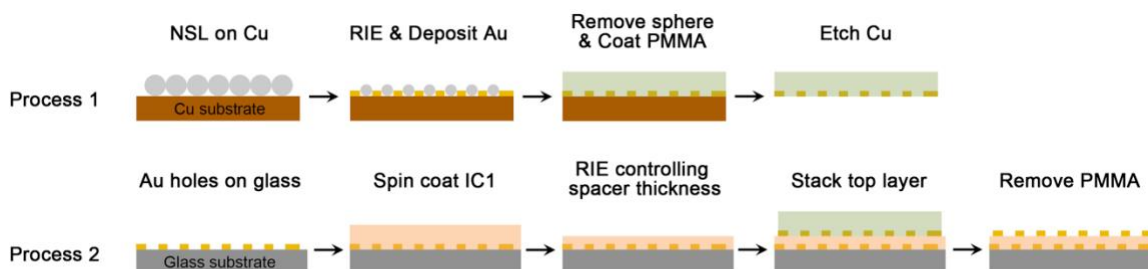

Figure S4. Schematics of fabrication steps for a moiré chiral metamaterial with a precisely controlled dielectric spacer layer thickness.
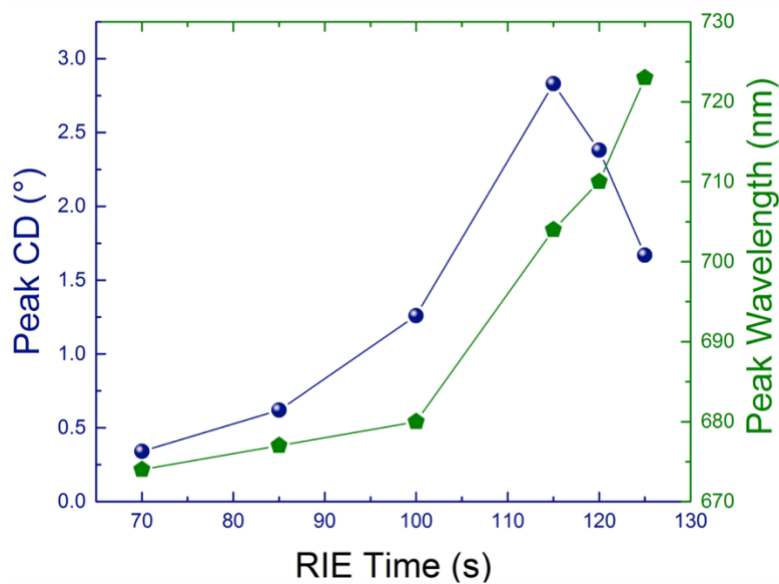
Figure S5. RIE time tunes the peak wavelength and CD value of the CD spectra of the RH MCMs by controlling the spacer thickness.

6. Silk-MCMs

6.1 Fabrication of silk-MCMs

The fabrication process was like the procedures shown in Figure S4. The slight difference was in the preparation of the spacer layer. As shown in the "Process 2" in Figure S6, silk fibroin solution was spin-coated onto the Au nanohole arrays on the glass substrate. A subsequent immersion of the whole substrate in methanol for 1 min crosslinked the silk fibroin to form a hydrogel-like silk thin film. A second layer of Au nanohole arrays from "Process 1" was transferred onto the silk spacer to form the silk-MCM.
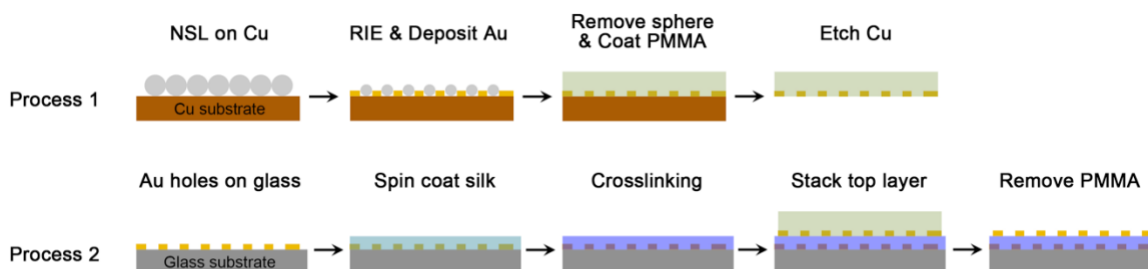
Figure S6. Schematics of the fabrication steps for a silk-MCM.

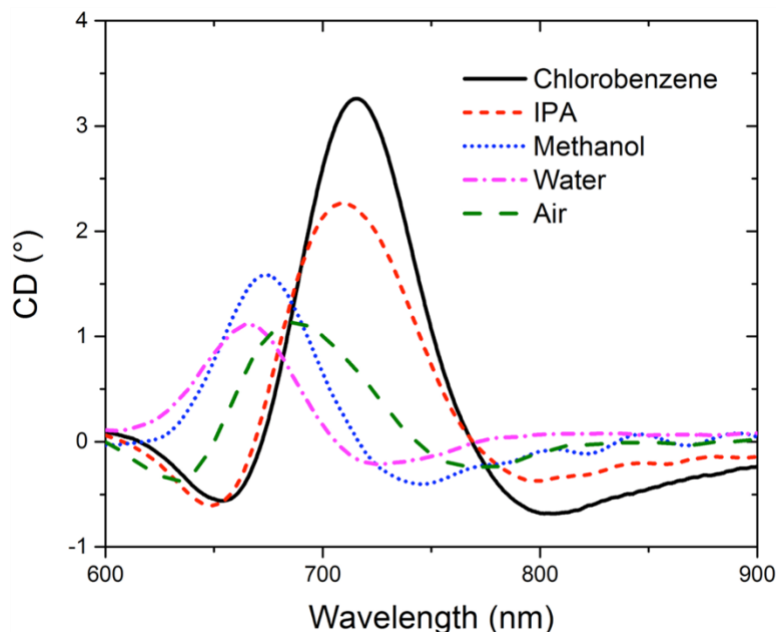6.2 CD spectra of silk-MCMs exposed to the various solvents

Figure S7. Measured CD spectra of the RH silk-MCM exposed to the various solvents with the different polarities. The CD spectrum of the RH silk-MCMs in air is also shown.

7. ON/OFF Switching of Color Contrast in Silk-MCMs

To demonstrate the ON/OFF switching of color contrast in the silk-MCMs, we used a digital camera, in combination with a 650 nm long pass filter, to take optical images of an area on the sample that contain both enantiomers (i.e., LH and RH) of the silk-MCMs and an achiral region, as shown in the upper-left panel of Figure S8. Such an area was readily available due to the polycrystallinity of PS sphere monolayers. The achiral regions arose from the in-plane rotation angles of $n\pi/6$ between the two Au nanohole arrays, where n is an integer. As shown in the upper-left image in Figure S8, for the silk-MCM exposed to IPA and under LCP light illumination, the LH enantiomer appeared darker than both the RH enantiomer and the achiral region. Changing LCP to RCP light illumination made the RH enantiomer appear darker (down-left image in Figure S8). The color contrast arose because the LH and RH enantiomers had the largest CD values around a wavelength of 708 nm when the silk-MCM was exposed to IPA. The color contrast was switched

OFF when the silk-MCM was exposed to water, which led to a CD value of ~0 around the wavelength of 708 nm (right-column images of Figure S8). The reversible ON/OFF switching of the color contrast was achieved by an alternative exposure of the silk-MCMs to IPA and water.
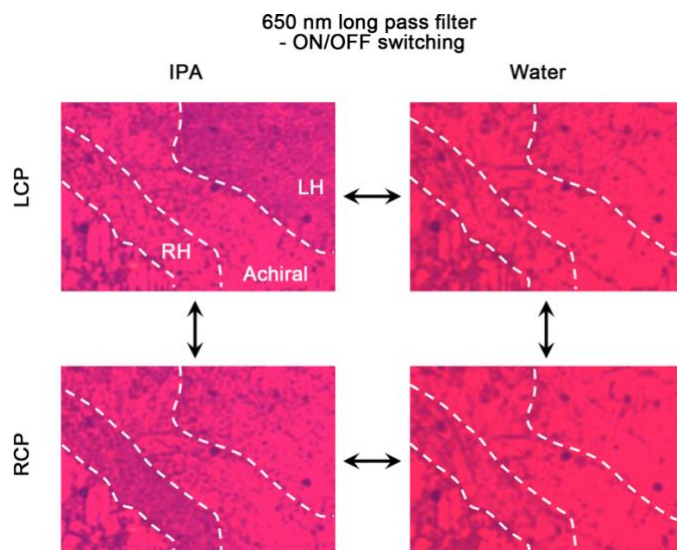

Figure S8. Reversible ON/OFF switching of color contrast between LH and RH enantiomers of the silk-MCMs under LCP (or RCP) light illumination and alternatively exposed to water and IPA.

8. Visualizing Inversion of Chiroptical Responses of Silk-MCMs

To visualize inversion of chiroptical responses of the silk-MCMs, we used a digital camera combined with a 650 nm short pass filter to take the gray-scale optical images. As shown in Figure S9, when the silk-MCM was exposed to IPA and illuminated by RCP light, the RH enantiomer appeared brighter than the LH enantiomer because the RH enantiomer had positive CD values between 600 nm and 650 nm. Similar but opposite color contrast can be observed when illuminating the MCMs with LCP light. When replacing the IPA by water, the CD signs below 650 nm inversed.

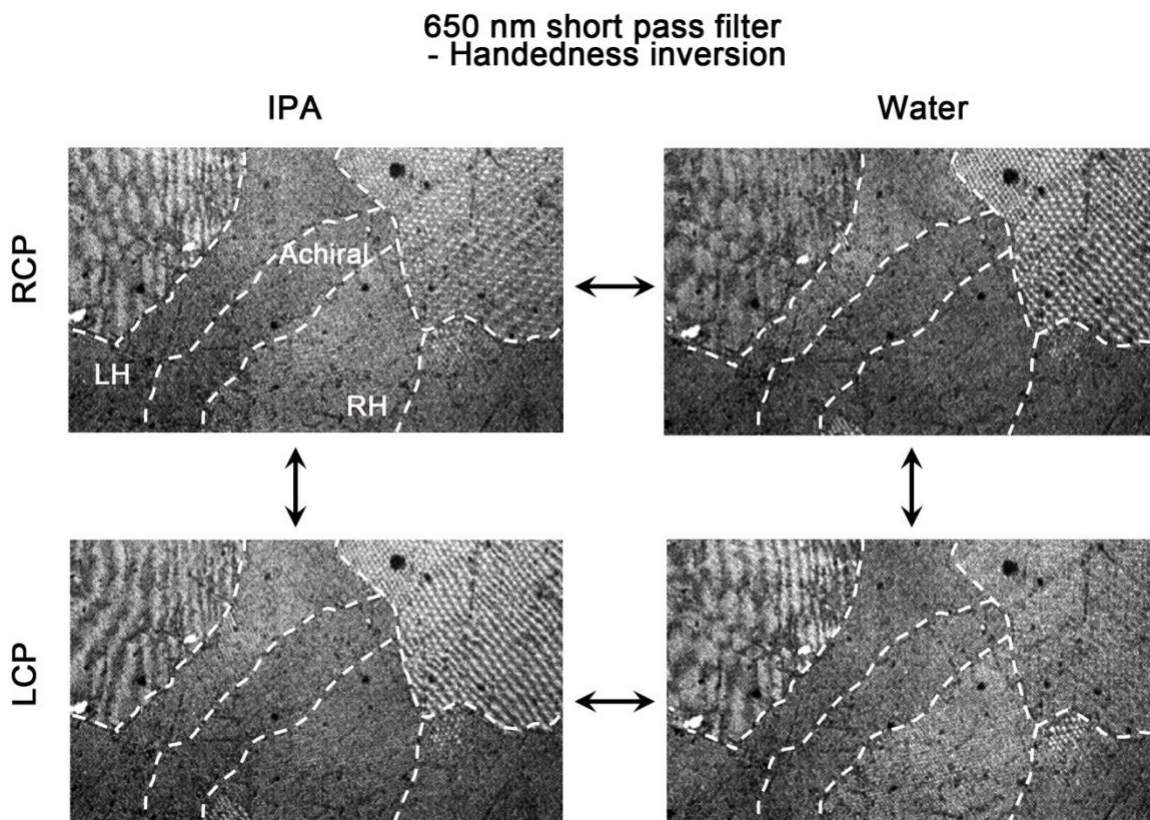**650 nm short pass filter - Handedness inversion**

Figure S9. Grey-scale optical images, which were recorded by a digital camera combined with a 650 nm short pass filter, enable us to visualize the active handedness inversion in the chiroptical responses of the silk-MCMs when alternatively exposed to water and IPA.

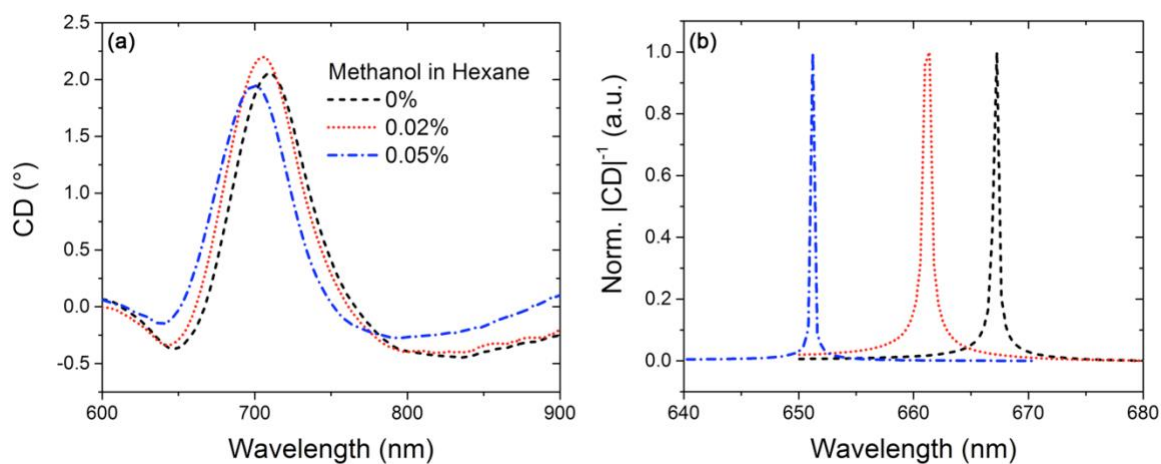## 9. Ultrasensitive Detection of Trace Amounts of Methanol in Hexane.

Figure S10. Ultrasensitive detection of trace amounts of methanol in hexane. (a) CD spectra of the

RH silk-MCM subsequently exposed to pure hexane and methanol-hexane mixtures with 0.02% (200 ppm) and 0.05% (500 ppm) methanol in volume. (b) Normalized zoom-in $|CD|^{-1}$ spectra around the zero-crossing points in (a).

References

1. Gallinet, B.; Martin, O. J. F., Influence of Electromagnetic Interactions on the Line Shape of Plasmonic Fano Resonances. *ACS Nano* **2011,** *5* (11), 8999-9008.

2. Kelly, C.; Khosravi Khorashad, L.; Gadegaard, N.; Barron, L. D.; Govorov, A. O.; Karimullah, A. S.; Kadodwala, M., Controlling Metamaterial Transparency with Superchiral Fields. *ACS Photonics* **2017**.

3. Garcia-Vidal, F. J.; Martin-Moreno, L.; Ebbesen, T. W.; Kuipers, L., Light passing through subwavelength apertures. *Rev. Mod. Phys.* **2010,** *82* (1), 729-787.

4. de León-Pérez, F.; Brucoli, G.; García-Vidal, F. J.; Martín-Moreno, L., Theory on the scattering of light and surface plasmon polaritons by arrays of holes and dimples in a metal film. *New Journal of Physics* **2008,** *10* (10).